



Superior Adsorption Property of a Novel Green Biosorbent Yttrium/Alginate Gel Beads for Dyes from Aqueous Solution

Beigang Li^{1,2} · Haiyang Yin^{1,2}

Published online: 1 July 2020
© Springer Science+Business Media, LLC, part of Springer Nature 2020

Abstract

A novel biosorbent yttrium/sodium alginate (Y/SA) hydrogel was prepared by the crosslinking of sodium alginate (SA) and yttrium (Y) ions and characterized by Scanning Electron Microscopy (SEM) and Energy Dispersive Spectroscopy (EDS), X-ray Diffraction (XRD), Fourier Transform-Infrared (FTIR), UV visible diffuse reflectance spectroscopy (UV–Vis DRS) and Thermogravimetric Analysis (TGA), respectively. The important parameters affecting the adsorption of Congo Red (CR) and Weak Acid Brilliant Blue RAW (WABB RAW) onto Y/SA were investigated systematically, respectively. The results show that Y/SA gel beads have super-strong adsorption performance for CR and WABB RAW dyes in a wide pH range of 2.0–10.0. The equilibrium data fitted by Langmuir and Freundlich models were found to completely follow Langmuir model where the obtained maximum adsorption capacities of 1567 and 1087 mg/g for CR and WABB RAW were very close to the experimental adsorption capacities, respectively, showing the adsorption of monomolecular layer. The adsorption kinetic data of two dyes by Y/SA fully accorded with the pseudo-second-order rate equation and adsorption processes were mainly controlled by intraparticle diffusion. The results of thermodynamic study indicate the feasible, spontaneous and exothermic nature of adsorption reaction. The further study revealed that electrostatic adsorption, hydrogen bonding and ion exchange reaction were the predominant adsorption for dye removal from aqueous solution by Y/SA gel beads. As a highly efficient, green and conducive to solid–liquid separation biosorbent, Y/SA hydrogel has great potential-application prospects for the purification of high-concentration dyestuff effluent.

Keywords Sodium alginate · Yttrium ions · Biosorbent · Adsorption · Dyes

Introduction

A large number of synthetic dyes have been widely used in various industrial production, such as textile printing and dyeing, dyeing of leather, paper, plastic, printing ink, cosmetics, food, etc., but more than 15% of them are lost as waste liquid [1]. The dyes with complex aromatic ring structure are difficult to be degraded, and have potential toxicity and side effects. When the industrial waste liquid containing these high-concentration dyes is discharged into nearby water body, it will not only seriously affect the

photosynthesis of aquatic organisms due to its deep color, disturb and damage to the normal aquatic environment, but also cause harm to human health [2]. As an anionic dye with diazo structure, Congo red (CR) has carcinogenicity and mutagenicity [3, 4]. Weak acid brilliant blue RAW (WABB RAW) is also an anionic dye with anthraquinone structure, which is commonly used for dyeing wool, silk, nylon and their blends, etc. Due to the environmental side of their structure, color and concentration, the effluent liquor containing these dyes must be effectively treated before discharge. In common wastewater treatment technologies, adsorption technology is considered one of the most economical and effective methods owing to its simple process, convenient operation and high efficiency. So a large number of related studies have been reported in recent years [5, 6]. The key of adsorption method depends on the selection of adsorbent. High-effect adsorbent can not only reduce the investment and operation cost of treatment process, but also usefully improve the treatment efficiency. Traditional

✉ Beigang Li
libeigang_1964@126.com

¹ Chemistry & Environment Science College, Inner Mongolia Normal University, Hohhot 010022, People's Republic of China

² Inner Mongolia Key Laboratory of Environmental Chemistry, Hohhot 010022, People's Republic of China

adsorbents, activated carbon, zeolite and so on, have disadvantages of high treatment cost and limited adsorption capacity, which will limit their popularization and application [7, 8]. Therefore, based on the characteristics of different dye-discharged wastewater, the development projects about adsorbents with abundant sources and low costs like some industrial wastes, agricultural by-products and biosorbents, have been widely performed for removing dyes from aqueous solutions at present [9–12].

Sodium alginate (SA) is a natural polysaccharide ionic polymer from algae, which has many advantages of biosafety, biocompatibility, no-toxicity, regeneration and abundant resources. SA has strong hydrophilicity and can react with polyvalent cations to form polymer gel beads [13, 14]. This property makes SA an ideal framework for preparing alginate gel beads and alginate-based composite adsorbents [15]. A large number of –OH and –COOH groups on the linear molecular chain of SA can adsorb metal ions and organic pollutants from industrial effluent through coordination, ion exchange and electrostatic interaction. Hence, the preparation and adsorption application of environmentally-friendly alginate-based gel composites have been extensively studied in recent years [16–18].

Based on the special electronic layer structure of rare-earth elements, the high charge of their ions and coordination to oxygen, and the coagulation effect of rare-earth salts, the research and application of rare earths in the preparation of water treatment materials have attracted more and more attention in recent years. The exchange reactions between rare-earth ions and ligands are very fast in solution. Therefore, the combination of rare-earth ions with organic polymers and rare-earth metal-based composite adsorbents can play a synergistic role and maximize the adsorption and coagulation effect [19–21].

In this study, biopolymer yttrium(III)/alginate (Y/SA) gel beads were prepared and used to remove Congo Red (CR) and Weak Acid Brilliant Blue RAW (WABB RAW) dyes in wastewater respectively. The effects of some important factors on the adsorbent performance were explored through a series of adsorption experiments. The performance and adsorption mechanism of the adsorbent were evaluated by

the characterization of materials, adsorption kinetics and isothermal studies. We hope that this environment-friendly biosorbent can have superb adsorption capacities for anionic dyes in high-concentration industrial wastewater.

Materials and Methods

Materials

Sodium alginate (SA, A.R.) and Yttrium nitrate hexahydrate ($Y(NO_3)_3 \cdot 6H_2O$, A.R.) were purchased from Shandong Xiya Chemical Industry Co., Ltd. and Tianjin Guangfu Fine Chemical Research Institute, China, respectively. Congo Red (CR, $C_{32}H_{22}N_6O_6S_2Na_2$, relative molecular mass $M_r = 696.68$ g/mol) and Weak Acid Brilliant Blue RAW (WABB RAW, $C_{22}H_{28}N_2O_8S_2Na_2$, $M_r = 678.68$ g/mol) dyes were bought from Shanghai Jiaying Chemical Co., Ltd., China. The maximum adsorption wavelength (λ_{max}) of CR and WABB RAW are at 498 nm and 566 nm, respectively. Their molecular structures are presented in Fig. 1.

Preparation and Characterization of Y/SA Biopolymer

The optimum process for preparation of Y/SA gel beads was as follows (in Fig. 2): the uniformly stirred 2 g/100 mL SA solution was dripped slowly into 4 g/100 mL $Y(NO_3)_3$ solution through the syringe at 25 °C, and the Y/SA gel beads were gradually generated. After crosslinking reaction for 2 h, the milk-white gel beads were removed, washed and dried, finally the beige Y/SA biosorbent was obtained.

The surface feature and elemental distribution of SA and Y/SA gel beads were characterized using scanning electron microscopy and energy dispersive spectroscopy (SEM–EDS, SU8010, Hitachi Inc., Japan). The molecular structures and crystallinity of materials were analyzed by a Nicolet Nexus 6700-type Fourier transform infrared spectrometer (FTIR, KBr tableting method, Thermo Fisher Scientific Inc., U.S.A), UV-2550 ultraviolet visible diffuse reflection spectrometer (UV–Vis DRS, Shimadzu

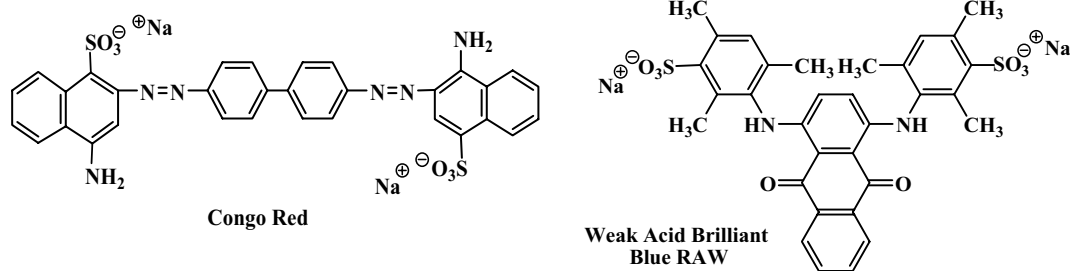
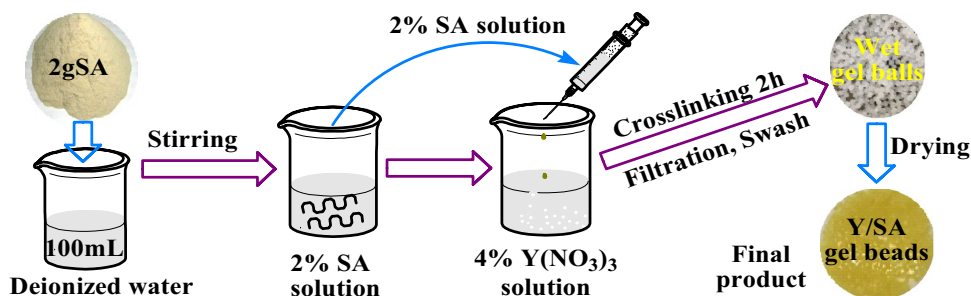


Fig. 1 The chemical structures of two dye molecules

Fig. 2 Preparation process of Y/SA gel beads



Inc., Japan) and a PW-1830 X-ray diffractometer (XRD, Philips, Holland) by applying monochromated Cu K α radiation ($\lambda=0.154056$ nm) in the 2θ range of $5\text{--}80^\circ$. Thermal stability of materials was investigated by DTG-60H Thermogravimetric analyzer (TGA, Shimadzu Inc., Japan).

Adsorption Tests

In order to investigate the adsorption efficiency of dyes onto Y/SA in detail, a series of adsorption experiments were carried out including optimization of adsorption conditions, adsorption kinetics and isothermal adsorption tests. A 0.05 g adsorbent was added to 25 mL dye solution with a certain concentration and oscillated to the adsorption equilibrium at 160 rpm and a fixed temperature. The dye concentration in a solution after adsorption was determined at the maximum wavelength (498 nm and 566 nm) of dye on an UV/Vis spectrophotometer (U-2900E, Japan), respectively. The linear regression equations of the standard curves used for the determination of dye concentration are as follows: $A = 0.0223C + 0.0027$ and the correlation coefficient $R^2 = 0.9998$ for CR, and $A = 0.0148C + 0.068$ and $R^2 = 0.9999$ for WABB RAW, respectively. Through 11 parallel blank determinations, the obtained detection limits of CR and WABB RAW are 0.27 and $0.20\mu\text{g/mL}$, respectively. The adsorption capacity (Q_e , mg/g) and removal efficiency (R , %) of dyes by adsorbent are calculated from the following formulas, respectively.

$$Q_e = (C_0 - C_e) \times V/m \quad (1)$$

$$R\% = (C_0 - C_e)/C_0 \times 100 \quad (2)$$

where C_0 and C_e are the dye concentration (mg/L) in a solution before and after adsorption, respectively. V (L) is the volume of each dye solution and m (g) is the adsorbent dosage. For each sample, three parallel determinations were completed. The mean value, whose relative standard deviation was controlled below 0.2%, was used as the result for analysis.

Determination on Point of Zero Charge (pHpzc)

To further understand the charged properties of adsorbent surface, the point of zero charge (pHpzc) of Y/SA was measured according to the following method. A 0.01 mol/L NaCl solution of 10 mL was added to a series of 50 mL conical flasks. The pH value of each solution was adjusted in the range of 2.0–12.0 (named as pH_0), and 0.05 g Y/SA biosorbent was added in each solution. After 24 h of continuous oscillation at 25°C , the series of mixed solution were withdrawn and the pH of each solution was again determined (named as the pH^*). The relation curve of ΔpH ($\text{pH}_0 - \text{pH}^*$) versus pH_0 was plotted, and the intersection point between ΔpH and pH_0 was the point of zero charge (pHpzc) of Y/SA adsorbent.

Results and Discussion

Characterizations of SA and Y/SA Materials

The surface morphology and element distribution of SA powder and Y/SA gel beads were analyzed by SEM and EDS (in Fig. 3). It is seen from Fig. 3a that SA is composed of irregular particles with different sizes. Figure 3b shows that the wet Y/SA gel beads synthesized in the solution are milky white translucent spheres with a diameter of about 3 mm. After drying, Y/SA gel beads turned to beige spheres with a diameter of about 1 mm. The surface of each gel ball emerges irregular deep grooves and wrinkles. This is due to the ion exchange between Y(III) ions and a large number of Na^+ in SA molecules, and further crosslinking of SA molecular chain with Y(III) ions, resulting in the formation of polymer gel beads with three-dimension network structure and unique surface morphology. The polymer adsorbent with such structure is very conducive to the improvement of its adsorption performance and solid–liquid separation. It is found from the EDS analysis of Fig. 3d that the content of Na element in Y/SA is significantly lower than that in SA (Fig. 3c). There is not Y element in SA (Fig. 3c), but its content in Y/SA increases significantly, indicating that most

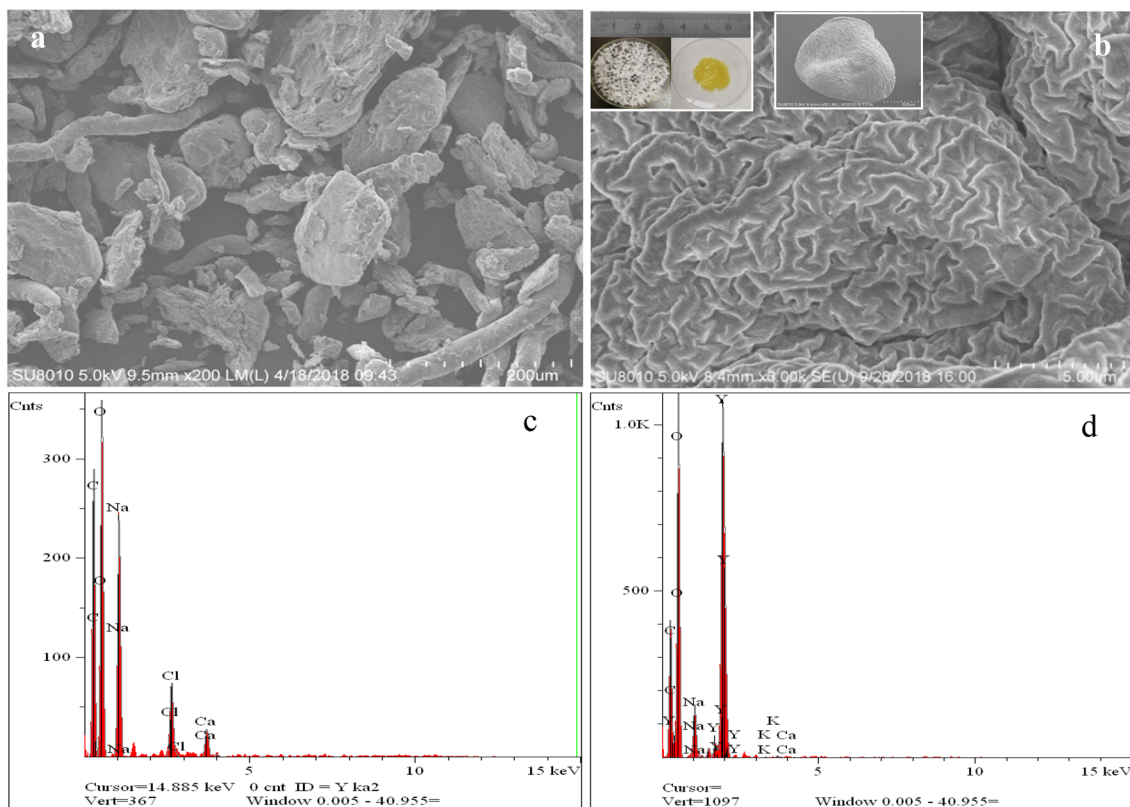


Fig. 3 SEM images of SA (a) and Y/SA (b) and corresponding analytical results by EDS (c and d)

of Na^+ ions in SA molecules was exchanged by Y(III) ions and Y/SA biosorbent was successfully synthesized.

XRD Patterns

The crystal structures of SA and Y/SA biopolymer analyzed by XRD are given in Fig. 4a. The characteristic diffraction peaks of SA were respectively at $2\theta = 13.5^\circ$ and 23° , and there was a large steamed bread peak in the 2θ range of 10° – 30° . Similar results was also been reported in relevant literature [22]. Compared with the XRD patten of SA, the two broad new characteristic peaks appearing around $2\theta = 17.5^\circ$ and 38.3° represented the formation of yttrium alginate in the XRD diagram of Y/SA, further confirming that the formation of Y/SA gel beads completely changed the crystalline structure of SA.

FTIR Analysis

Figure 4b shows the FTIR spectra of SA and Y/SA. The characteristic absorption bands for SA are assigned as follows: 3440 cm^{-1} ($-\text{OH}$ stretching vibration), 2930 cm^{-1} ($-\text{CH}$ stretching vibration), 1631 and 1404 cm^{-1} (the asymmetric and symmetric stretching peaks of $-\text{C}=\text{O}$ and $-\text{COO}^-$), 1033 cm^{-1} ($\text{C}-\text{O}-\text{C}$ stretching vibration) [21,

23]. Compared with FTIR spectra of SA, the characteristic peak of $-\text{COO}^-$ group disappeared in Y/SA spectra, but sharper absorption peak appeared near 1384 cm^{-1} . The stretching vibration peak of $\text{C}-\text{O}-\text{C}$ was moved from 1033 to 1038 cm^{-1} . Other absorption peaks also changed in intensity [21]. The variation of these characteristic peaks further confirmed that Y(III) ions reacted with the $-\text{COO}^-$ groups on SA molecules and formed water-borne gel beads, and the oxygen between the rings on SA molecular chain also participated in the polymerization reaction.

UV-Vis DRS Analysis

It can be observed from the UV-Vis DRS spectra of Fig. 4c that the spectrum of SA has no absorption peak in the range of 200 – 800 nm , while that of Y/SA has two absorption peaks at 283 and 330 nm , respectively. This fully indicated that a new compound, namely Y/SA, was synthesized by the reaction of SA and Y ion(III).

Thermogravimetric Analysis (TGA)

To know the thermal stability of SA and Y/SA better, the thermogravimetric analysis of SA and Y/SA was carried out and the results are given in Fig. 4d. With the rise of

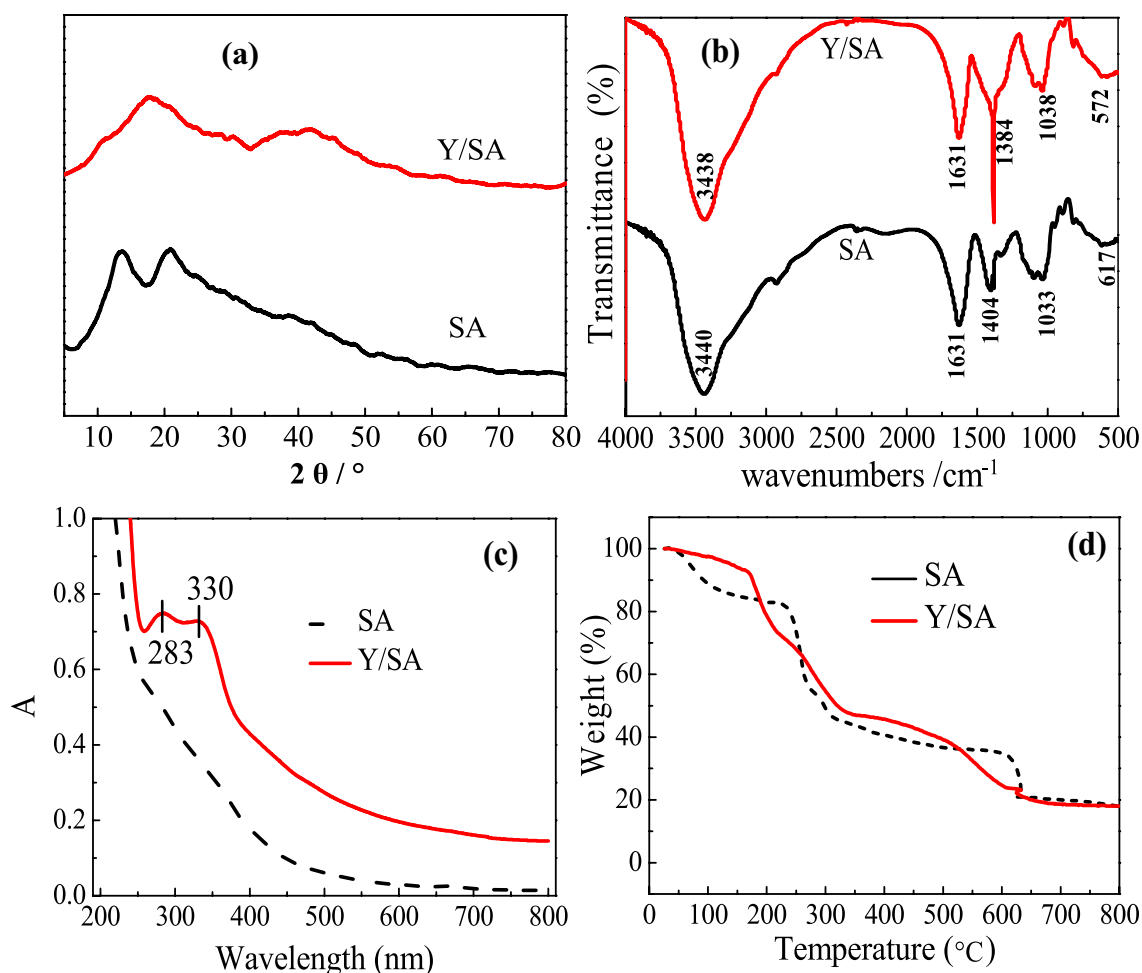


Fig. 4 XRD patterns (a), FTIR (b), UV–Vis DRS (c) analysis and TGA (d) of SA and Y/SA

temperature, the change of Y/SA mass mainly underwent three stages of decline. The rate of mass decline was slow before 180 °C, and the Y/SA mass decreased by 21% due to the evaporation of free water and bound water. The sample underwent a rapid decomposition stage from 200 to 350 °C, and the mass reduced by 31%. The thermal decomposition rate slowed down gradually in the range of 350 to 600 °C and then entered a relatively stable state after 600 °C. However, the decomposition rate of SA was very fast before 100 °C. The results of TGA analysis illustrate that the stability of Y/SA is significantly better than that of SA, and Y/SA adsorbent with good thermal stability before 150 °C is more convenient to store and use in ordinary temperature.

Effect of Solution pH and Adsorbent Dosage

The water acidity is one of the most important factors affecting the adsorbent performance. The effect of initial solution pH on the adsorption of CR and WABB RAW by Y/SA is shown in Fig. 5a. When the pH of dye solution

was 2.00, the adsorption capacity (Q_e) and removal rate ($R\%$) reached the maximum values with 1500 mg/g and 100% for CR and 980 mg/g and 98% for WABB RAW, respectively. When the pH value increased from 2.0 to 10.0, the values of Q_e and R only decreased slightly. The removal rates of CR and WABB RAW could still reach 95% and 91% at pH = 10.0, respectively, suggesting that Y/SA has excellent adsorption performance in a wide range of pH and can be used for highly efficient treatment of dye effluent with different acidity and alkalinity. After the solution pH was greater than 10.0, the values of Q_e and R decreased rapidly. The highly pH-dependent adsorption is primarily related to the surface properties of Y/SA polymer and species of dyes. CR and WABB RAW dye molecules exist as anions in solution because of containing two $-\text{SO}_3^-$ groups in each molecule. The positive charge density on the surface of Y/SA increases with the reduction of solution pH owing to the protonation of rich $-\text{OH}$ groups and the existence of Y(III) ions with high positive charge on Y/SA gel beads. The point

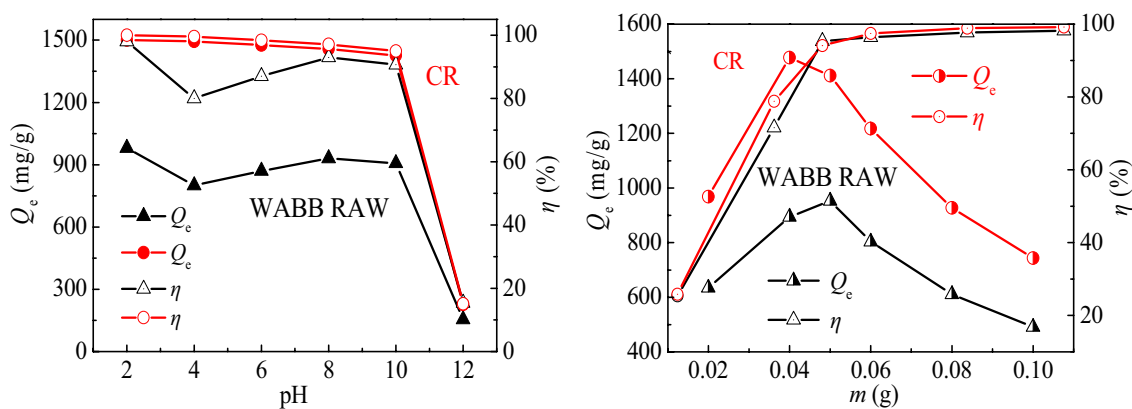


Fig. 5 The effect of solution pH (a); Effect of adsorbent dosage on the adsorption (b)

of zero charge (pHpzc) of Y/SA was determined to be around 6.15, indicating that the surface of Y/SA is positively charged at $\text{pH} < \text{pHpzc}$, which resulted in strongly electrostatic adsorption between Y/SA and dye anions. In contrast, the surface of gel ball is negatively charged at $\text{pH} > \text{pHpzc}$ which generated electrostatic repulsion between adsorbent and the dye anions and reduced the adsorption capacity. However, the Q_e values of two dyes decreased significantly after $\text{pH} > 10.0$, which indicated that there were other adsorption effects such as hydrogen bonding and ion exchange in the pH range of 6.15–10.0. The pH values of actual CR and WABB RAW dye solutions are about 9.5 and 7.0, respectively, so the acidity of dye solutions does not need to be adjusted and can be directly treated with Y/SA adsorbent, making the adsorption operation easier, faster and more efficient.

The effect of Y/SA dosage on the removal of CR and WABB RAW dye with 3000 and 2000 mg/L initial concentrations respectively is presented in Fig. 5b. For dye solutions with fixed mass concentration, the dosage of adsorbent directly affects the adsorption capacities and removal rates of dyes. Figure 6b shows that the adsorption capacities of two dyes on Y/SA increase first and then diminish with the increase of adsorbent dosage, but the removal rates of dyes increase rapidly at first and then slowly, so the platforms appear at the upper parts of the curves. When the adsorbent dosage was 0.04 g, the adsorption capacity of Y/SA for CR reached the maximum value of 1478 mg/g, but the removal rate was only 79%. When the adsorbent dosage was 0.05 g, the adsorption capacity for WABB RAW reached the maximum value of 953 mg/g and the corresponding removal rate can exceed 95%, and the removal rate of CR can also exceed 94%. Considering the adsorption efficiency and the convenience of practical operation, the dosage of Y/SA adsorbent was chosen to be 0.05 g.

Adsorption Kinetic and the Effect of Temperature

The process of dye adsorption is mainly accomplished in two steps: the first step is the diffusion of dye anions from solution to adsorbent surface, and the second step is the migration and adsorption reaction from the outer surface to the inner surface of adsorbent particles. However, the change of adsorption rate given by different processes is totally different, which is also related to the adsorption temperature. In order to investigate the adsorption kinetics and the effect of temperature on it, the adsorption amount was plotted as a function of time for CR and WABB RAW, respectively, as shown in Fig. 6a and b. It can be seen clearly from Fig. 6a and b that the adsorption rates of two dyes were very fast, and the adsorption amounts reached 1326 mg/g and 880 mg/g in 30 min and accounted for more than 88% of the total dye removal rates. Afterwards the adsorption rate slowed down obviously. The fast adsorption kinetics of dye-Y/SA system is very beneficial to the actual wastewater treatment because of the shortening of adsorption equilibrium time, the improvement of treatment efficiency and the reduction of operation cost. The adsorption of two dyes was in kinetic equilibrium after 90 min.

In addition, It was found from Fig. 6a and b that the increase in temperature from 298 K to 328 K caused a significant decrease in the adsorption rate of CR, especially after 30 min of adsorption. However, the adsorption of WABB RAW evidently increased with the increase of temperature before 30 min as shown in Fig. 6b, thereafter, the influence of temperature was very little, even the value of Q_t decreased slightly, especially after adsorption equilibrium. It shows that room temperature is beneficial to the effective equilibrium adsorption of two dyes. Considering the adequacy of adsorption, 120 min of adsorption equilibrium time were selected for further study, and the adsorption capacities of CR and WABB RAW dyes can

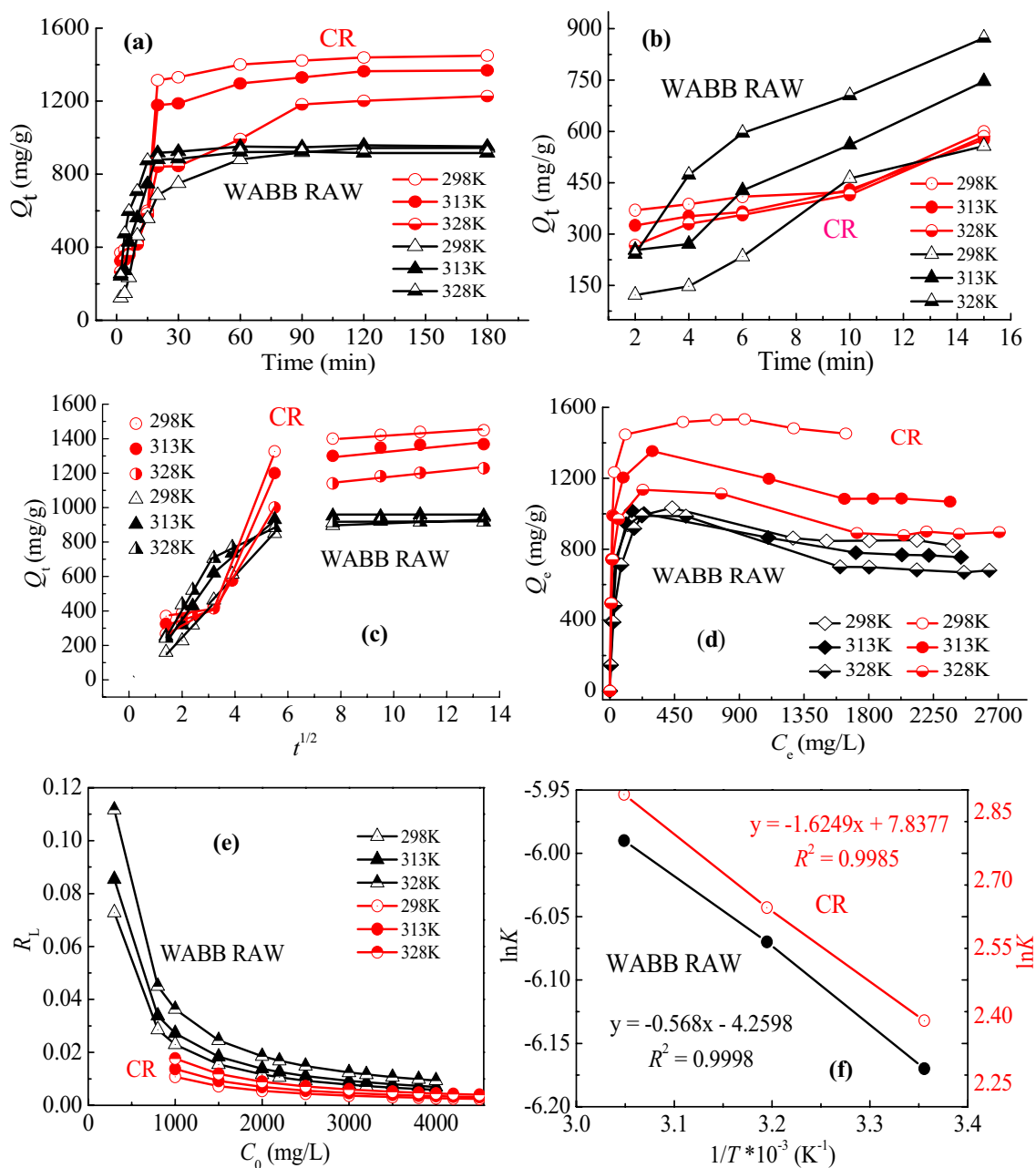


Fig. 6 The effect of contact time and temperature (a and b) on the adsorption; The plot of Q_t versus $t^{1/2}$ (c); Adsorption isotherms of dyes on Y/SA (d); The plot of R_L versus C_0 (e); The plot of $\ln K$ versus $1/T$ (f)

reach 1439 and 943 mg/g with removal rates of 95.9 and 94.3%, respectively.

Moreover, the adsorption capacity of CR by Y/SA was significantly higher than that of WABB RAW in equilibrium (Fig. 6a). This difference may be mainly due to the fact that CR molecule contains more active groups, such as two $-NH_2$ groups and $-N=N-$ groups, than WABB RAW molecule, which made the interaction between CR anion and adsorbent stronger. At the same time, it was also related to dimensions of dye organic chain [24].

The experimental data at different temperatures were processed using the pseudo-first-order, pseudo-second-order rate models and intraparticle diffusion model respectively to clarify the kinetic mechanism of adsorption process, and the corresponding expressions are as follows [25–27], respectively.

$$\log(Q_e - Q_t) = \log Q_e - k_1 t \tag{3}$$

$$\frac{t}{Q_t} = \frac{1}{k_2 Q_c^2} + \frac{t}{Q_c} \tag{4}$$

$$Q_t = K_p t^{1/2} \tag{5}$$

where k_1 and k_2 are the rate constants of pseudo-first-order and pseudo-second-order models, min^{-1} and $\text{g}/(\text{mg}\cdot\text{min})$, respectively. K_p is the intraparticle diffusion rate constant, $\text{mg}/(\text{g}\cdot\text{min}^{1/2})$. Some parameters, the correlation coefficients (R^2) and the error values including sum of squared errors (SSE) and root mean squared error (RMSE) [2, 28] obtained by pseudo-first-order and pseudo-second-order kinetic models are listed in Table 1. It can be known from Table 1 that the pseudo-second-order rate model for the adsorption of two dyes shows a better fit ($R_2^2 > 0.999$) to the experimental data than the pseudo-first-order model ($R_1^2 > 0.854$) at different temperatures (298–328 K). The pseudo-first-order model is suitable for the initial fast adsorption stage due to a large concentration difference between the adsorbent surface and the solution. This also elucidates that the whole adsorption processes of two dyes onto Y/SA are not only controlled

by external mass transfer. However, the adsorption of both fast and slow processes fits well with the pseudo-second-order model, which indicates that the adsorption of two dyes occurs through internal and external mass transfer mechanism. The equilibrium adsorption capacities ($Q_{e,2}$) are close to the experimental values, showing that the adsorption of CR and WABB RAW onto Y/SA occurred by the mechanisms of liquid film diffusion, pore migration and monolayer buildup of adsorption [29].

To identify the rate-limiting steps for the whole adsorption process of CR and WABB RAW onto Y/SA, according to Eq. (5), fitted data of Q_t versus $t^{1/2}$ and the Weber and Morris plots present the three distinct linearity in Fig. 6c and Table 1, respectively. All regression lines do not pass the origin. The values ($R_1^2 > 0.939$ and $R_2^2 > 0.983$) of the correlation coefficient in the initial part (2–10 min) and the second part (10–30 min) indicate that the intraparticle diffusion is a rate-limiting step, but not the only one. This further elucidates that both liquid film diffusion and intraparticle diffusion occur simultaneously. The third part is a dynamic adsorption equilibrium stage after 60 min as shown in Fig. 6c.

Table 1 Correlation coefficients and some parameters fitted by different kinetics models

Dye	T (K)	$Q_{e,\text{exp}}$ (mg/g)	Pseudo-first-order			Error values	
			k_1 (min^{-1})	$Q_{e,1}$ (mg/g)	R_1^2	SSE	RMSE
CR	298	1449	0.0420	56.5	0.9683	0.964	0.121
	313	1368	0.0415	56.2	0.9964	0.120	0.0150
	328	1228	0.0375	61.4	0.9915	0.182	0.0223
WABB RAW	298	944	0.0408	56.5	0.9893	0.398	0.0498
	313	937	0.0395	59.9	0.9449	1.912	0.239
	328	917	0.0305	56.8	0.9359	3.385	0.423
Dye	T (K)	$Q_{e,\text{exp}}$ (mg/g)	Pseudo-second-order			Error values	
			k_2 [$\text{g}/(\text{mg}\cdot\text{min})$]	$Q_{e,2}$ (mg/g)	R_2^2	SSE	RMSE
CR	298	1449	0.0015	1518	0.9994	1.78×10^{-5}	3.56×10^{-6}
	313	1368	0.0016	1396	0.9991	2.98×10^{-5}	3.72×10^{-6}
	328	1228	0.0017	1318	0.9994	1.87×10^{-5}	2.34×10^{-6}
WABB RAW	298	944	0.0023	1000	0.9993	2.18×10^{-5}	2.73×10^{-6}
	313	937	0.0023	994	0.9995	1.60×10^{-5}	2.29×10^{-6}
	328	917	0.0025	909	0.9996	1.57×10^{-5}	1.97×10^{-6}
Dye	T (K)	Intraparticle diffusion model					
		First stage (2~10 min)		Second stage (10~30 min)			
		K_p ($\text{mg}/\text{g}\cdot\text{min}^{1/2}$)	C	R_1^2	K_p ($\text{mg}/\text{g}\cdot\text{min}^{1/2}$)	C	R_2^2
CR	298	38.6	314	0.9677	403	910	0.9864
	313	39.3	271	0.9885	344	711	0.9853
	328	90.2	143	0.9853	254	393	0.9998
WABB RAW	298	154	63.5	0.9567	164	48.3	0.9837
	313	169	5.64	0.9394	133	205	0.9945
	328	282	146	0.9879	76.9	462	0.9970

Adsorption Isotherms

The relationship between adsorption capacity (Q_e) and equilibrium concentration (C_e) of dyes between solid and liquid phases at adsorption equilibrium is given in Fig. 6d. The adsorption capacities of two dyes on Y/SA decrease with increasing temperature from 298 to 328 K, especially in the high concentration regions in Fig. 6d. This is consistent with the effect of temperature on adsorption kinetics, illustrating that room temperature is more conducive to the highly efficient adsorption. The adsorption behavior has been commonly described using two models, namely Langmuir and Freundlich models, whose linear equations are expressed as follows:

$$\frac{C_e}{Q_e} = \frac{C_e}{Q_m} + \frac{1}{Q_m K_L} \tag{6}$$

$$\ln Q_e = \ln K_F + \frac{1}{n} \ln C_e \tag{7}$$

$$R_L = 1/(1 + K_L C_0) \tag{8}$$

where Q_m is the maximum adsorption capacity, mg/g; K_L is the Langmuir adsorption coefficient, L/mg; K_F and n are the Freundlich empirical constants, respectively; R_L is called a separation factor defined by Langmuir model. The fitting results, correlation coefficients (R^2) and the values of sum of squared error (SSE) and root mean squared error (RMSE) of all equilibrium data of CR and WABB RAW adsorption on Y/SA fitted by the two models are listed in

Table 2. The Langmuir model was in good agreement with the equilibrium data for the CR and WABB RAW adsorption ($R^2 > 0.99$) and the values of $Q_{e,exp}$ were very close to those of Q_m , suggesting the dye adsorption of monomolecular layer and the existence of chemical adsorption. The values of K_L diminished with rise in temperature, affirming the exothermic nature of dye adsorption which agreed with the kinetic results. The maximum adsorption capacities of CR and WABB RAW on Y/SA can reach 1567 and 1000 mg/g at 298 K, respectively.

Some studies on adsorbing performance of various materials for CR and the corresponding maximum adsorption capacities have been reported [3, 30–41], which are listed in Table 3. Compared with various adsorption materials presented in Table 3, Y/SA biosorbent shows more significant advantages and higher cost-effectiveness for CR adsorption, and has simpler preparation methods and greater potential for popularization and application as a superior green adsorbent.

The value of separation factor R_L can judge whether the adsorption type is favorable ($0 < R_L < 1$) or unfavorable ($R_L > 1$). It is observed from Fig. 6e that all values of R_L for the adsorption of two dyes were in the range of 0.0024–0.112, confirming to be favorable for the adsorption of CR and WABB RAW on Y/SA. However, adsorption data of two dyes on Y/SA did not have a good fit for Freundlich model ($R^2 > 0.629$). This may be because the Freundlich adsorption model is an empirical model, which refers to multi-layer adsorption. Nevertheless, the values of n less than 10 from Freundlich model (in Table 2) also show the advantage of adsorption reaction.

Table 2 Fitting results of two isotherm models for equilibrium data and thermodynamic parameters of dye adsorption

Dyes	T (K)	Langmuir model					Freundlich model				
		Q_m (mg/g)	K_L (L/mg)	R^2	SSE	RMSE	n	K_F	R^2	SSE	RMSE
CR	298	1567	0.0916	0.9999	2.66×10^{-4}	2.95×10^{-5}	6.38	544	0.7290	4.45	0.495
	313	1414	0.0717	0.9997	0.00186	2.33×10^{-4}	5.98	448	0.7854	4.12	0.515
	328	1000	0.0556	0.9994	0.00933	0.00140	5.79	405	0.7804	4.00	0.444
WABB RAW	298	1087	0.0425	0.9996	0.00621	6.21×10^{-4}	4.42	210	0.6297	0.219	0.0243
	313	1000	0.0357	0.9981	0.0423	0.00470	3.57	175	0.6597	3.72	0.413
	328	1000	0.0265	0.9993	0.0156	0.00174	3.24	140	0.6957	3.36	0.373
Dyes	T (K)	Thermodynamic parameters									
		ΔG° (kJ/mol)	ΔH° (kJ/mol)	ΔS° (kJ/mol·K)							
CR	298	-32.9	- 13.5	0.065							
	313	-33.9									
	328	-34.5									
WABB RAW	298	-33.3	- 12.7	0.069							
	313	-34.3									
	328	-35.0									

Table 3 Comparison of the maximum adsorption capacity of CR adsorbed by different adsorbents

Adsorbents	Maximum adsorption capacity obtained from isotherm model (mg/g)	Reference
Diacrylamidobenzoic acid based hyper-cross-linked resin	252.1	[3]
Hierarchical flower-like NiO microspheres	534.8	[30]
Palygorskite-template amorphous carbon nanotubes	467.97	[31]
Coal-based mesoporous activated carbon	189	[32]
Metal hydroxide sludge	271	[33]
Kaolin	1.98	[34]
Na-Bentonite	35.84	[34]
Red mud	4.05	[35]
Chitosan/montmorillonite nanocomposite	54.52	[36]
Raw pine	32.65	[37]
Acid-treated pine cone powder	40.19	[37]
AC from grape processing waste	455	[38]
AC from waste pine cone	500	[39]
ACF from silkworm cocoon	512	[40]
Ni/Mg/Al layered double hydroxides (NMA-LDHs)	1250	[41]
Yttrium/alginate (Y(III)/SA) gel beads	1567	This study

Adsorption Thermodynamics

According to van't Hoff equation and the dependence of Langmuir adsorption coefficient (K_L) on temperature (T , K), the standard Gibbs free energy change (ΔG° , kJ/mol), standard enthalpy change (ΔH° , kJ/mol) and entropy change (ΔS° , kJ/mol·K) can be calculated by the Eqs.(9) and (10) [42].

$$\ln K = -\frac{\Delta H^\circ}{RT} + \frac{\Delta S^\circ}{R} \quad (9)$$

$$\Delta G^\circ = \Delta H^\circ - T\Delta S^\circ \quad (10)$$

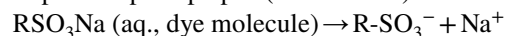
The linear curve of $\ln K$ versus $1/T$ is presented in Fig. 6f and the values of ΔH° and ΔS° calculated by the slope and intercept and ΔG° are given in Table 2. The negative values of ΔG° and ΔH° for CR and WABB RAW dyes revealed the spontaneous and exothermic nature of adsorption reaction. The positive values of ΔS° indicated the increase of confusion degree on solution-gel beads interface. This might be owing to the release of large amounts of water molecules hydrated on the gel beads surface through substitution of dye macromolecules.

Discussion on Adsorption Mechanism

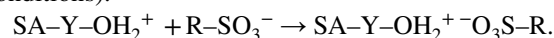
To explore the interaction between Y/SA adsorbent and dye molecules, the FTIR and UV-Vis DRS spectra of Y/SA before and after adsorbing CR and WABB RAW are

presented in Fig. 7. The main changes in the spectra of Y/SA after dye adsorption in Fig. 7a are that the sharp stretching vibration peaks at 1384 cm^{-1} almost disappear, while the new absorption peaks appear at 1404 cm^{-1} and 1410 cm^{-1} , respectively. The intensity or position of other characteristic peaks also varies slightly. These changes fully explain the interaction between Y/SA gel beads and dye molecules. The significant changes of the UV-Vis DRS spectra of Y/SA after dye adsorption were shown in Fig. 7b. The original two absorption peaks disappeared and two new absorption peaks appeared at 349 and 504 nm for Y/SA-CR and at 312 and 603 nm for Y/SA-WABB RAW, respectively, and the absorption peaks became wider, further proving the interaction between Y/SA and dye molecules.

Combined with the results of material characterization and adsorption studies, it might be considered that the adsorption of CR and WABB RAW dyes onto Y/SA gel beads was mainly accomplished by strong electrostatic adsorption at $\text{pH} < \text{pHpzc}$ (around 6.15) as follows:



$\text{SA-Y-OH} + \text{H}^+ \rightarrow \text{SA-Y-OH}_2^+$ (Under acidic conditions).



When the solution pH was in the range of 6.15–10.0, the adsorption of dye anions onto Y/SA gel beads was first related to the ion-exchange reaction between hydroxyl groups bonded to yttrium (Y-OH) and dye anions (R-SO_3^-) as shown in Fig. 8 [21], then to the hydrogen bonding of multiple sites between dye anions with $-\text{NH}_2$, $-\text{N}=\text{N}-$ and $-\text{SO}_3^-$ functional groups and Y/SA polymer with rich $-\text{OH}$

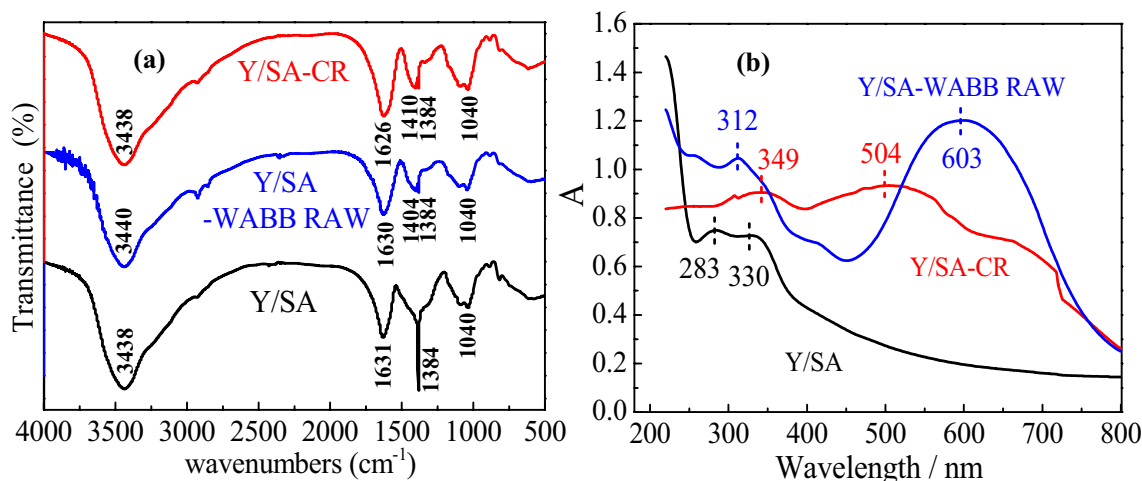
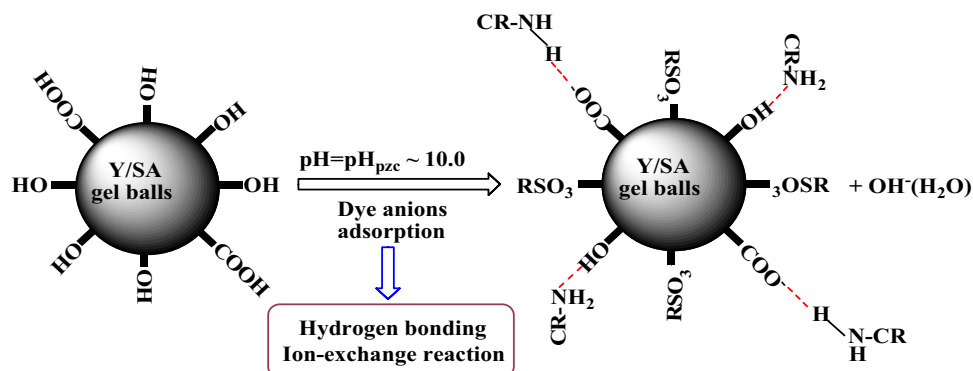


Fig. 7 The FTIR (a) and UV-Vis spectra (b) of Y/SA before and after adsorbing dyes

Fig. 8 Diagrammatic sketch of dye anion adsorption on Y(III)/SA



and -COOH groups (in Fig. 8) [3, 31]. In addition, the adsorption capacity of Y/SA adsorbent for CR was larger than that for WABB RAW. This may be due to the fact that there are still two -NH_2 groups and -N=N- groups in CR molecules, which can have more binding sites to interact with the adsorbent than WABB RAW, except for two sulfonic groups in both dye molecules.

Conclusions

The biosorbent Y/SA gel beads synthesized by droplet polymerization using SA as raw material and Yttrium ions as crosslinker exhibited a superior adsorption performance for direct dye CR and acidic dye WABB RAW from aqueous solutions. Through the study of some important factors affecting the adsorption, it is found that the adsorbent Y/SA has ultrahigh adsorption capacity and removal efficiency for two dyes in a wide pH range of 2.0–10.0. The analysis of experimental kinetic data revealed that the adsorption processes of two dyes nicely followed the pseudo-second-order rate model ($R^2 > 0.999$) and were significantly controlled by

the intraparticle diffusion in the fast adsorption stage. The good fitting of equilibrium data for Langmuir model in the given adsorption systems ($R^2 > 0.998$) indicated the monolayer formation of dye adsorption onto Y/SA gel beads, and the obtained maximum adsorption capacities were 1567 mg/g for CR and 1087 mg/g for WABB RAW at 298 K, respectively. The results of thermodynamics study interpreted the spontaneous and exothermic properties of dye adsorption. The results of spectral characterization of the adsorbent before and after dye adsorption and the adsorption research indicated that the adsorption between Y/SA adsorbent and dye molecules mainly included electrostatic adsorption, hydrogen bonding and ion exchange reaction. As a very promising and important alternative material, the novel high-efficiency biosorbent Y/SA gel beads with ultrahigh adsorption capacity would be used for the treatment of high-concentration dyes effluent.

Acknowledgements This study was funded by the National Natural Science Foundation of China (21167011), the Inner Mongolia Natural Science Foundation (2015MS0226) and the Inner Mongolia Normal University Science Research Foundation (112129K18ZZYF006).

References

1. Tharaneedhar V, Senthil Kumar P, Saravanan A, Ravikumar C, Jaikumar V (2017) *Sustain Mater Technol* 11:1
2. Anitha T, Senthil Kumar P, Sathish Kumar K (2016) *J Water Process Eng* 13:127
3. Waheed A, Mansha M, Kazi IW, Ullah N (2019) *J Hazard Mater* 369:528
4. Senthil Kumar P, Ramalingam S (2013) *Int J Ind Chem* 4:17
5. Sienkiewicz A, Kierys A, Goworek J (2019) *J Disper Sci Technol* 40:1396
6. Grace Pavithra K, Senthil Kumar P, Jaikumar V, Sundar Rajan P (2019) *J Ind Eng Chem* 75:1
7. Rashidi NA, Yusup S (2017) *Chem Eng J* 314:277
8. Hadi P, Xua M, Ning C, Lin CSK, McKay G (2015) *Chem Eng J* 260:895
9. De Gisi S, Lofrano G, Grassi M, Notarnicola M (2016) *Sustain Mater Technol* 9:10
10. Liu QM, Li YY, Chen HF, Lu J, Yu GS, Möslang M, Zhou YB (2020) *J Hazard Mater* 382: <https://doi.org/10.1016/j.jhazmat.2019.121040>
11. Zhang L, Sellaoui L, Franco D, Dotto GL, Bajahzar A, Belmabrouk H, Bonilla-Petriciolet A, Oliveira MLS, Li Z (2019) *Chem Eng J* 372: <https://doi.org/10.1016/j.cej.2019.122952>
12. Senthil Kumar P, Sivaranjane R, Vinothini U, Raghavi M, Rajasekar K, Ramakrishnan K (2013) *Desalin Water Treat* 51:1
13. Cho E, Kim J, Park CW, Lee K-W, Lee TS (2018) *J Hazard Mater* 360:243
14. Eskhan A, Banat F (2018) *J Polym Environ* 26:2901
15. Chiew CSC, Poh PE, Pasbakhsh P, Tey BT, Yeoh HK, Chan ES (2014) *Appl Clay Sci* 101:444
16. Agnihotri S, Singhal R (2019) *J Polym Environ* 27:372
17. Benhouria A, Islam MA, Zaghouane-Boudiaf H, Boutahala M, Hameed BH (2015) *Chem Eng J* 270:621
18. Kumar M, Dosanjh HS, Singh H (2018) *J Inorg Organomet P* 28:1688
19. Xu QY, Chen ZB, Wu ZS, Xu F, Yang DX, He Q, Li G, Chen Y (2019) *Bioresour Technol* 289:1
20. Zhang SY, Lyu Y, Su XS, Bian YY, Yu BW, Zhang YL (2016) *Environ Earth Sci* 75:401
21. He JS, Cui AN, Ni F, Deng SH, Shen F, Yang G (2018) *J Colloid Interface Sci* 531:37
22. Fabryanty R, Valencia C, Soetaredjo FE, Putro JN, Santoso SP, Kurniawan A, Ju YH, Ismadji S (2017) *J Environ Chem Eng* 5:5677
23. Wei L, Hong TQ, Liu HB, Chen TH (2017) *J Cryst Growth* 113:60
24. Cestari AR, Vieira EFS, Santos AGP, Mota JA, Almeida VP (2004) *J Colloid Interface Sci* 280:380
25. Lagergren S (1898) *K Sven Vetenskapsakad Handl* 24:1
26. Ho YS, McKay G (1999) *Process Biochem* 34:451
27. Weber JW, Morris JC (1963) *J Sanit Eng Div* 89:31
28. Jothirani R, Senthil Kumar P, Saravanan A, Narayan Abishek S, Abhishek D (2016) *J Ind Eng Chem* 39:162
29. Dotto GL, Pinto LAA (2011) *J Hazard Mater* 187:164
30. Zheng Y, Zhu B, Chen H, You W, Jiang C, Yu J (2017) *J Colloid Interface Sci* 504:688
31. Zhong L, Tang A, Yan P, Wang J, Wang Q, Wen X, Cui Y (2019) *J Colloid Interface Sci* 537:450
32. Lorenc-Grabowska E, Gryglewicz G (2007) *Dyes Pigm* 74:34
33. Golder A, Samanta A, Ray S (2006) *Chem Eng J* 122:107
34. Vimonses V, Lei S, Jin B, Chow CWK, Saint C (2009) *Chem Eng J* 148:354
35. Namasivayam C, Arasi D (1997) *Chemosphere* 34:401
36. Wang L, Wang A (2007) *J Hazard Mater* 147:979
37. Dawood S, Sen TK (2012) *Water Res* 46:1933
38. Saygili H, Güzel F (2015) *Chem Eng Res Des* 100:27
39. Dawood S, Sen TK, Chi P (2014) *Water Air Soil Pollut* 225:1818
40. Li J, Ng DHL, Song P, Kong C, Song Y, Yang P (2015) *Biomass Bioenerg* 75:189
41. Lei C, Zhu X, Zhu B, Jiang C, Le Y, Yu J (2017) *J Hazard Mater* 321:801
42. Tellinghuisen J (2006) *Biophys Chem* 120:114

Publisher's Note Springer Nature remains neutral with regard to jurisdictional claims in published maps and institutional affiliations.